J Mater Sci (2009) 44:5197–5204
DOI 10.1007/s10853-009-3626-1

FERROELECTRICS

Imaging domains in $BaTiO_3$ single crystal nanostructures: comparing information from transmission electron microscopy and piezo-force microscopy

L. McGilly · D. Byrne · C. Harnagea · A. Schilling · J. M. Gregg

Received: 25 March 2009 / Accepted: 19 May 2009 / Published online: 2 June 2009

Abstract This article compares and contrasts information obtained, using transmission electron microscopy (TEM) and piezo-force microscopy (PFM), on domain configurations adopted in single crystal lamellae of $BaTiO_3$, that had been cut directly from bulk using a focused ion beam microscope with top and bottom surfaces parallel to $\{100\}_{pseudocubic}$. Both forms of imaging reveal domain walls parallel to $\{110\}_{pseudocubic}$, consistent with sets of 90° domains with dipoles oriented parallel to the two $<001>_{pseudocubic}$ directions in the plane of the lamellae. However, the domain width was observed to be dramatically larger using PFM than it was using TEM. This suggests significant differences in the surface energy densities that drive the domain formation in the first place, that could relate to differences in the boundary conditions in the two modes of imaging (TEM samples are imaged under high vacuum, whereas PFM imaging was performed in air). Attempts were made to map local dipole orientations directly, using a form of 'vector' PFM. However, information inferred was largely inconsistent with the known crystallography of the samples, raising concern about the levels of care needed for accurate interpretation of PFM images.

L. McGilly · D. Byrne · A. Schilling · J. M. Gregg (✉)
Centre for Nanostructured Media, School of Maths and Physics, Queen's University Belfast, Belfast BT7 1NN, Northern Ireland, UK
e-mail: m.gregg@qub.ac.uk

C. Harnagea
University of Quebec, INRS Energy, Materials & Telecommunication, Varennes PQ J3X 1S2, Canada

Introduction and motivation

Harnessing the local non-volatile electric fields generated at the surfaces of ferroelectrics, for the manipulation and control of charge in modern electronic devices, looks to be an extremely attractive proposition. This is clearly illustrated, for example, by the recent development of Ferroelectric Random Access Memories (FeRAMs) [1] and the projected hopes for Ferroelectric Field-Effect Transistors (FeFETs) [2, 3]. In both applications, switching the orientation of dipoles within the ferroelectric is an important aspect of function. Such dipolar switching relies on the creation and growth of domains, and so to fully appreciate and evaluate the potential for ferroelectrics in various electronic devices, it is important to study domain behaviour. This is particularly true at the nanoscale, partly because of its practical relevance in the context of component miniaturisation, and partly because domains become significantly smaller as specimen size is reduced. In fact, the number of domains per unit volume in nanoscale ferroelectric objects is significantly greater than in bulk [4–8], and hence their influence over functional behaviour becomes increasingly important as miniaturisation progresses. Moreover, theoretical studies suggest that the nature of domains themselves can radically change, with as yet unseen dipole vortex structures expected to evolve in an attempt to minimize the depolarising fields which become increasingly important as sizes are reduced [9].

In light of the above, the authors and co-workers have recently been involved in a programme to map and rationalize the domain structures that exist in ferroelectric nanoshapes, cut directly from bulk single crystal using a focused ion beam microscope (FIB). To date, we have examined domain states in thin plates, or lamellae, nanorods, and nanodots of $BaTiO_3$ [8–12], using both

conventional transmission electron microscopy (TEM) and scanning transmission electron microscopy (STEM). Results suggest that there is an interesting interplay between the effects of surface tension [13], which induces the formation of shape-conserving 90° domain sets, and depolarising fields [9], which cause packets of 90° domains to alter their orientation. However, in all cases the dipole directions, or polarization vectors, within each domain have been inferred from the crystallographic orientation of domain walls. This method is not ideal as there can be more than one possible set of inferred polarisation directions consistent with a given TEM or STEM image. Further, the contrast mechanisms which result in such clear domain images under STEM (Fig. 1) are not well understood, and we are not entirely confident that this mode of imaging is capable of producing contrast which would allow for the identification of vortex domains should they be present.

For these reasons nanoscale domain mapping using Piezoresponse Force Microsopy (PFM), which in theory allows for the direct determination of local dipole orientations, was tried as an alternative to the TEM and STEM used to date. In this article, we present PFM images from thin plates or lamellae of single crystal $BaTiO_3$, compare the implications of the domain structures observed under PFM with those already seen under STEM, and examine the extent to which approximate 'vector' PFM can be used to allow local polarisation directions to be meaningfully determined.

Piezoresponse force microscopy (PFM)

PFM is an Atomic Force Microscopy variant in which a modulated voltage reference signal, $V(\omega) = V_{ac}\cos(\omega t)$ of frequency ω and amplitude V_{ac}, is applied to a sharp conductive probe and is brought into contact with the ferroelectric, giving rise to an oscillatory deformation of the sample surface, $d = d_0 + \mathrm{A}\ \cos(\omega t + \varphi)$, from the equilibrium position d_0, with amplitude A, and an associated phase difference φ, determined by alignment of electric field and polarisation orientation. The resulting cantilever movement is then detected by standard AFM optical deflection onto a photosensitive diode and the signal demodulated by means of a lock-in-amplifier (LiA). In practice, out-of-plane, and in-plane piezoresponse, denoted Vertical PFM (VPFM), and Lateral PFM (LPFM [14]), respectively, can be separated through use of a split quadrant photodiode detector arrangement in which signals originating from the vertical deflection and torsional bending of the cantilever can be distinguished. It is important to note that PFM does not directly map the polarisation orientations within a ferroelectric material but instead measures the material's local electromechanical response to the applied electric field, which can be described fully through the piezoelectric constitutive equations [15].

To find the local polarisation orientation, in any given domain, three orthogonal scans must be performed: one to measure the out-of-plane component (VPFM), and two to measure the in-plane components (L_xPFM & L_yPFM) so that each can be combined to fully reconstruct a 3D polarisation map in what is termed 'vector' PFM [16]. For the second in-plane component, the sample must actually be physically rotated through 90° for the completion of the measurement. Consideration has to be given to the non-trivial superposition of the orthogonal components as the piezoelectric tensor treatment and careful calibration must be taken into account. As a result of the strict conditions that have to be obeyed, only a few cases exist of the accurate implementation of Vector PFM [17, 18].

Many aspects, such as the non-local capacitive interaction from the cantilever, the electrostatic force between the surface and probe, and non-localised electric fields from the conical part of the tip can all contribute to artefacts and complexities in PFM image interpretation. A thorough analysis has been reported on these various additional complexities by Kalinin et al. [19]. Further complexity is revealed when one assesses the electric field emanating

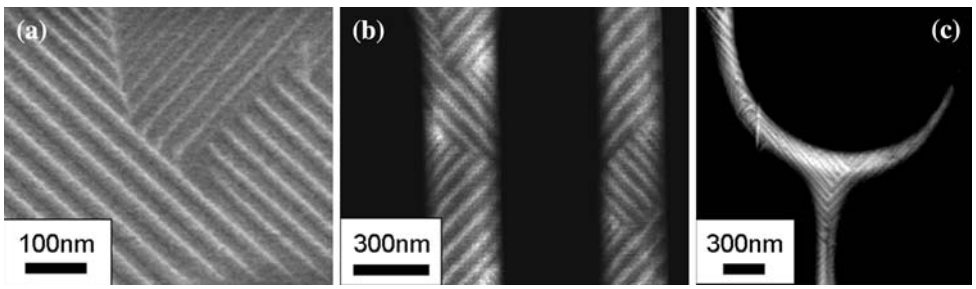

Fig. 1 Scanning transmission electron microscopy images of domain patterns in single crystal $BaTiO_3$ lamellae (**a**), rods (**b**) and rings (**c**). In all cases, domain walls were found to be parallel to $\{110\}_{pseudocubic}$ implying 90° domain sets. Such domains suggest that shape compensation is a major driving force in determining domain states in these nanostructures. However, previous studies [9–12] also show that depolarising fields have an influence

from the conductive probe and its associated electric displacement field within the material under examination [20]. A range of models have been used to describe this highly non-uniform field with various degrees of approximations, among which are point charge, sphere-plane, conical-plane, and conical with sphere apex-plane treatments. Together with these factors, the experimentalist has a range of external influences that can greatly affect the quality and even veracity of PFM imaging: cantilever spring constant and conductive material choice, indentation force, scan rate, and modulated-voltage amplitude and frequency all affect the tip-surface interaction; in addition, LiA time constant and sensitivity affect the collection of data, not to mention the usual inherent AFM technical complications such as scanner non-linearity, creep, drift, and tip wear, that all lead to the difficult implementation of successful, meaningful data acquisition. The optical detection system can also have a large influence on acquired data as reported by Huey et al. [21] as slight repositioning of the laser spot on the cantilever backside can even lead to inverted piezoresponse phase information. Overall, PFM can provide a bounty of information, but the data acquired must be continually questioned and assessed for undesired elements that can lead to data misinterpretation.

Experimental method

Commercially available polished single crystal barium titanate (BTO) was machined using a FEI 200TEM FIB microscope. The ion beam was oriented approximately parallel to the $[001]_{\text{pseudocubic}}$ crystallographic direction, to produce lamellar sheets of dimension $\sim 12 \times 10$ μm and thicknesses <200 nm with $\{001\}_{\text{pseudocubic}}$ bounding faces, as has been described in a previous study [22]. The lamellae were then removed from the bulk crystal using a sharp glass needle and a micromanipulator and placed either onto a clean single crystal Magnesium Oxide (MgO) substrate with a pre-deposited 100 nm film of platinum (as an electrode) for PFM, or onto carbon-coated copper grids for the TEM studies. Ion induced damage from the FIB machining resulted in a thin, ~20-nm deep, amorphous layer which needed to be recovered through thermal annealing in air or oxygen at 700 °C for 1 h. Such surface repair was critical for PFM imaging, and less critical for TEM; indeed, previous studies have shown that repair of ion implant damage does not affect the domain patterns imaged under TEM significantly [13].

Domains were imaged using a Tecnai F20 TEM with a high-angle annular dark field detector (HAADF) for STEM work, with the electron beam parallel to the $<100>_{\text{pseudocubic}}$ direction, i.e. approximately perpendicular to the lamellar faces. PFM characterisation was realised through use of a Veeco Dimension D3100 scanner with a Nanoscope IIIa controller and a Signal Recovery 7265 Lock-in-amplifier. Image size, scan rate, and LiA time constant were 20×20 μm^2, 0.1 Hz, and 5 ms, respectively and were constant for all the recorded images of resolution 256×256. All cantilevers used in this study (Nanosensors Pointprobe PPP EFM) have silicon tips coated with a Pt/Ir overlayer, with a force constant of $k_0 = 2.8$ Nm^{-1}. LiA demodulation resulted in a $R\cos(\theta)$ type output which contains the piezoresponse amplitude and phase information within a single voltage. Images were obtained in the three orthogonal scan configurations as necessary for vector PFM.

Results and discussion

Figure 2 shows the images associated with the vertical and two horizontal components of the PFM response for a $BaTiO_3$ lamella. Domain contrast is clearly evident, with domain walls oriented parallel to $\{110\}_{\text{pseudocubic}}$, consistent with the inferred existence of 90° domains taken from STEM images (Fig. 1a). However, the domain widths implied from PFM are dramatically coarser than those imaged in STEM, appearing to be around an order of magnitude larger. Previous studies [8–11] have shown that the domain period in ferroelectric nanoshapes follows a Kittel Law:

$$w^2 = \frac{\sqrt{2}}{2} \frac{\sigma}{\left(U_x/x + U_y/y + U_z/z\right)} \quad (1)$$

where x, y and z are the physical dimensions of the ferroelectric object in Cartesian space; U_x, U_y and U_z are surface energy densities for surfaces perpendicular to x, y and z, respectively; and σ is the energy density of the domain walls. For the one-dimensional case applicable to lamellae of constant thickness, z, the relation between domain periodicity and surface energy density can be expressed quite succinctly as

$$w^2 = \alpha \frac{1}{U_z} \quad (2)$$

Since the period of domains apparent in PFM are $\sim 10^1$ times larger than those under STEM imaging for the same thickness of lamella, the implication from Eq. 2, or any Kittel-like relation, is that the surface energy density of the lamellar surfaces when imaged under PFM is $\sim 10^2$ times smaller than when imaged under STEM. This is a dramatic change in the surface energy density.

There are obvious differences between the imaging conditions used in the two characterisation techniques: STEM is performed in a high vacuum environment where charge compensation is highly unlikely, whereas PFM is performed with a lower electrode (Pt thin film), conducting tip, and in an air ambient readily suspected to contain

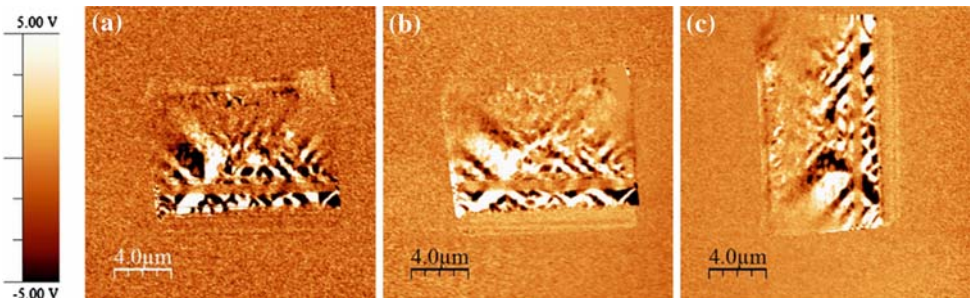

Fig. 2 Piezoresponse force microscopy images of a single crystal $BaTiO_3$ lamella on a platinised MgO substrate (imaging was performed using a tip voltage of 3 V_{rms}, and frequency of 23.6 kHz): VPFM (**a**); L_xPFM (**b**); and L_yPFM (**c**). The FIB machining process and subsequent annealing of the sample has resulted in gallium oxide island formation on the lamellar surface, leading to areas of reduced piezoresponse. Although domain wall orientation again implies 90° domain sets (consistent with STEM imaging), the apparent domain widths are dramatically increased. We note that in **c** an elongation can be seen along the vertical length of the image which corresponds to scanner non-linearity in the fast scan direction

adsorbates which can be highly effective in terms of charge compensation: Fong et al. [7] have shown that chemi-adsorbates can be even more compensating than electrode thin films whereas Wang et al. [23] have demonstrated that the chemical environment can reverse the polarisation orientation in $PbTiO_3$ thin films. However, differences in the charge compensation conditions at the free surfaces should only alter the domain periodicity if polarisation directions point out-of-the plane of the lamellae; the domain wall orientations observed in both STEM and PFM suggest that dipoles are oriented approximately in the plane of the lamellae, and in any case are 90° in nature suggesting that domain formation has been driven primarily by shape compensation and not in response to depolarising fields. Coarsening 90° domains, with in-plane polarisations, rather suggest that it is the effective surface tension associated with the lamellar surfaces that has changed by two orders of magnitude between STEM and PFM imaging conditions.

Let us now consider the potential for the PFM images to identify the polarisation directions within each domain. Interestingly, stripe domain structures were observed not only for the in-plane LPFM scans but also for the VPFM scan (Fig. 2). This is a puzzling result for {100} cut BTO lamellae in the tetragonal state, as polarisation can only exist in six possible directions: parallel and anti-parallel to each of the major crystallographic axes. The domain wall orientations and inferred in-plane domain structure do not allow for an out-of-plane component to be observed. Yet, domain contrast images are clearly observed by VPFM suggesting that this is likely to be an artefact of PFM scanning and not a physical representation of the domain structure, as would at first glance be assumed.

An explanation may come from the notion of crosstalk between VPFM and LPFM, an effect that has been reported elsewhere [16, 24] but is usually neglected on the grounds of its insignificant contribution. Take for example, a cantilever positioned over an in-plane domain in which a component of polarisation exists along the axis of the cantilever. An applied modulated voltage will excite the domain to oscillate such that longitudinal bending of the cantilever will result. As the detection system measures specifically an angle of deflection, rather than tip displacement, the resulting effect will be a mis-assignment of longitudinal translation of the tip to vertical electromechanical displacement, i.e. an apparent vertical polarisation component. Kalinin et al. [16] have considered this flexural effect and have produced a condition for artefact free VPFM scanning by analysis of the piezoresponse in two orthogonal scanning configurations, such that $\beta \ll 1$, where

$$\beta = \left(\frac{V_xPFM - V_yPFM}{V_xPFM + V_yPFM}\right) \tag{3}$$

V_xPFM and V_yPFM are used to describe the vertical piezoresponse signals in the non-rotated and 90° rotated configuration, respectively.

Overall, there have been relatively few studies on the degree to which LPFM and VPFM crosstalk can affect data interpretation, usually because of difficulties associated with scanning the same region after rotating the sample. In certain cases, when the desired region of the sample can be easily retrieved, the parameter β can be estimated and therefore the in-plane contribution to the VPFM signal can be assessed [25]. In our micron-scale lamellar $BaTiO_3$ samples, images from the same spatial region can unquestionably be retrieved upon rotating by 90 degrees. Consequently, two pertinent statements can be made: firstly, we have observed that, in many cases, the condition given in Eq. 3 is not met when imaging the $BaTiO_3$ lamellae. In fact, due to changes in phase in some areas between the orthogonal scans, the β factor implied can be greater than 10, pointing to a strong coupling of longitudinal in-plane surface deformation to vertical cantilever

deflection, i.e. high VPFM sensitivity to in-plane domain orientation. Secondly, we observe that L_xPFM image is identical with the V_yPFM image (Fig. 3). This definitely and indubitably confirms that the out-of-plane PFM signal originates from in-plane induced surface vibration.

Discounting the information from VPFM in this specific study, for the reasons given above, we then turned our attention to the much simpler case of 2D Vector PFM in which the in-plane components of PFM are combined to find the resultant local polarisation. This case should be particularly useful as from the domain wall orientations, we expect all local polarisations to lie in the plane of the lamella. Calibration of the two orthogonal components will be equivalent, as the imaging mode is the same, and the sample is simply rotated. Hence a vector sum of lateral PFM responses can be used to determine the resultant in-plane polar direction. Applying this to the L_xPFM and L_yPFM for the lamella illustrated in Fig. 4 reveals that the resolved resultant polarisation orientation vector lies at an angle that is strongly non-parallel to the lamellar edges. In fact, as the magnitudes of the L_xPFM and L_yPFM are comparable and in-phase, an approximate resolved polarisation vector implied is parallel to $<110>_{\text{pseudocubic}}$. This is more clearly elucidated in the complete in-plane polarisation vector PFM map illustrated in Fig. 5. Such polar directions are obviously non-physical. One is therefore faced with a conflict between the data obtained through simplified vector PFM, and the physical reality of possible polarisation directions of the system under examination.

A possible explanation for this observation could arise from a consideration of the limit of resolution in PFM. As is well known, the fundamental resolution is derived from the contact radius. However, for large scan areas, the effective limit in resolution will be related not to the contact radius but to user-defined parameters. This may well be a widely known fact, but it has not been explicitly reported to the authors' knowledge, and merits a brief discussion: A basic factor that must be considered is the pixel size of the PFM image; of course for large scans, the pixel size will be correspondingly large, e.g. for a 256×256 pixel image of scan size 20×20 μm each pixel will be of side 78 nm, so that features/structures smaller than this will not be entirely resolved. In general, for L being the length of one side of the scan area (i.e. one line) and N_s the number of samples per line (i.e. pixels) with distance between features, d, the above statement could be expressed as $\frac{L}{N_s} < d$ for features at scale d to be resolved.

Further, if we consider a tip in contact with a surface (and moving with velocity $v = 2LF$ ms^{-1} over a distance L at a scan frequency of F_{scan} (Hz)), the time, t, for the tip to move between features d apart is then $t = \frac{d}{2LF_{\text{scan}}}$. The LiA time constant, which determines the time over which the signal will be integrated to produce the output, is τ_{LiA} and

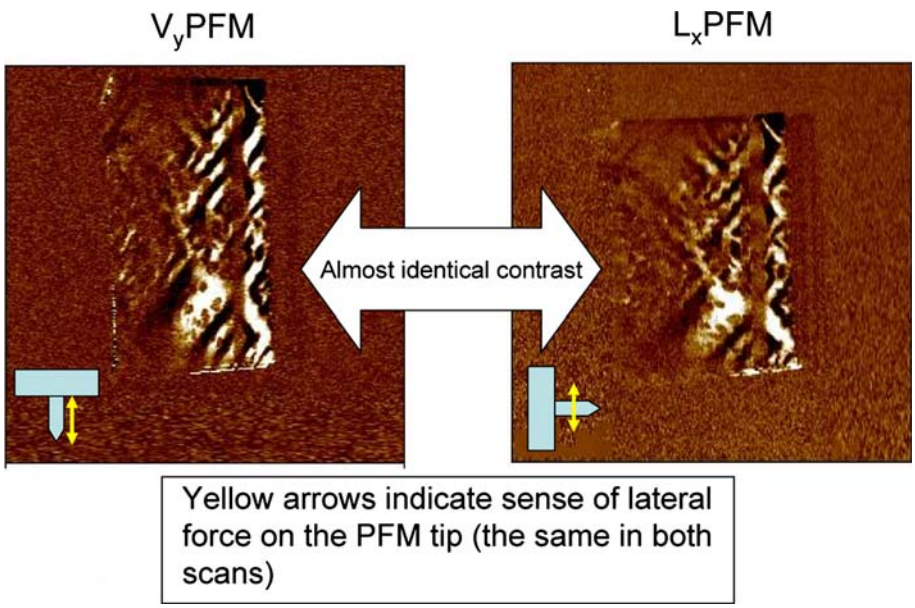

Fig. 3 Piezoresponse images which would usually correlate with vertical deflection of the cantilever (VPFM) appear, in this case, to be related to cantilever flexure, associated with in-plane tip–sample interactions. This is made clear by the identical contrast in the two images above—an interaction that causes tip rotation about an axis parallel to the cantilever axis results in contrast in the lateral PFM image on the right, but when the sample is rotated by 90°, the same tip–sample interaction now results in tip rotation about an axis perpendicular to the cantilever axis, and parallel to the sample surface (image on the left). This signal is then misinterpreted as an out-of-plane electromechanical coupling between tip and sample

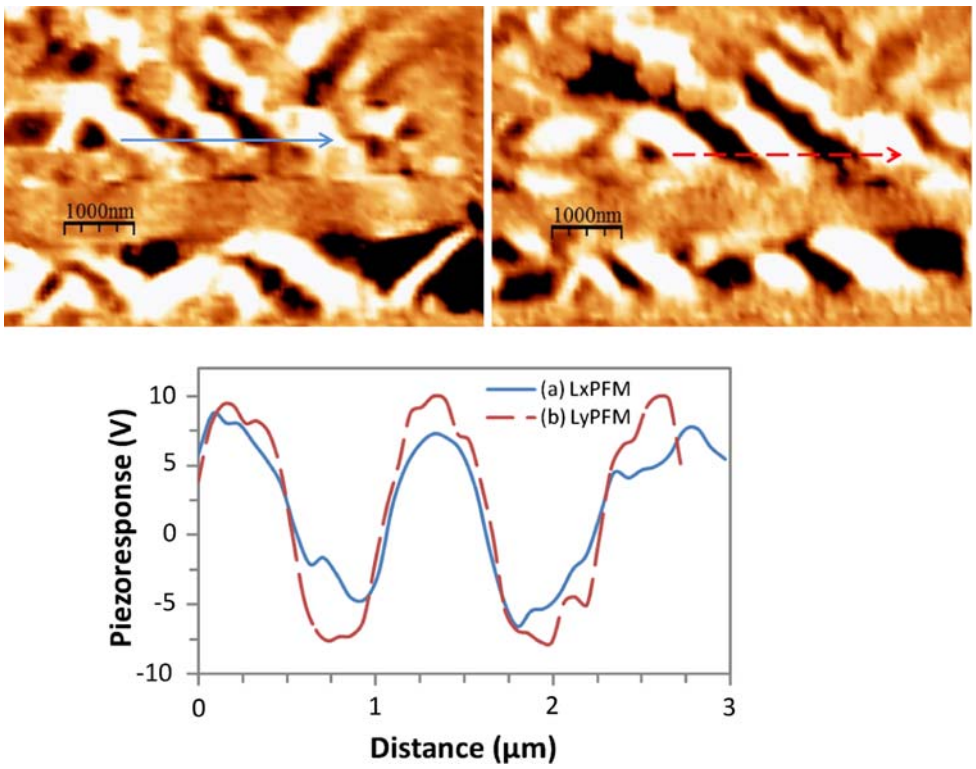

Fig. 4 Attempts to probe local polar orientation through 'vector' PFM using assumptions often used in literature (that the measured cantilever displacement is simply related to the direction of local polarisation) resulted in unphysical conclusions, given the known crystallographic orientation, and symmetry, of the $BaTiO_3$ lamella. The vector addition of in-plane PFM responses for the line sections highlighted clearly indicates a resultant polarisation which is not parallel to $<100>_{pseudocubic}$. In fact it looks to be approximately parallel to $<110>_{pseudocubic}$

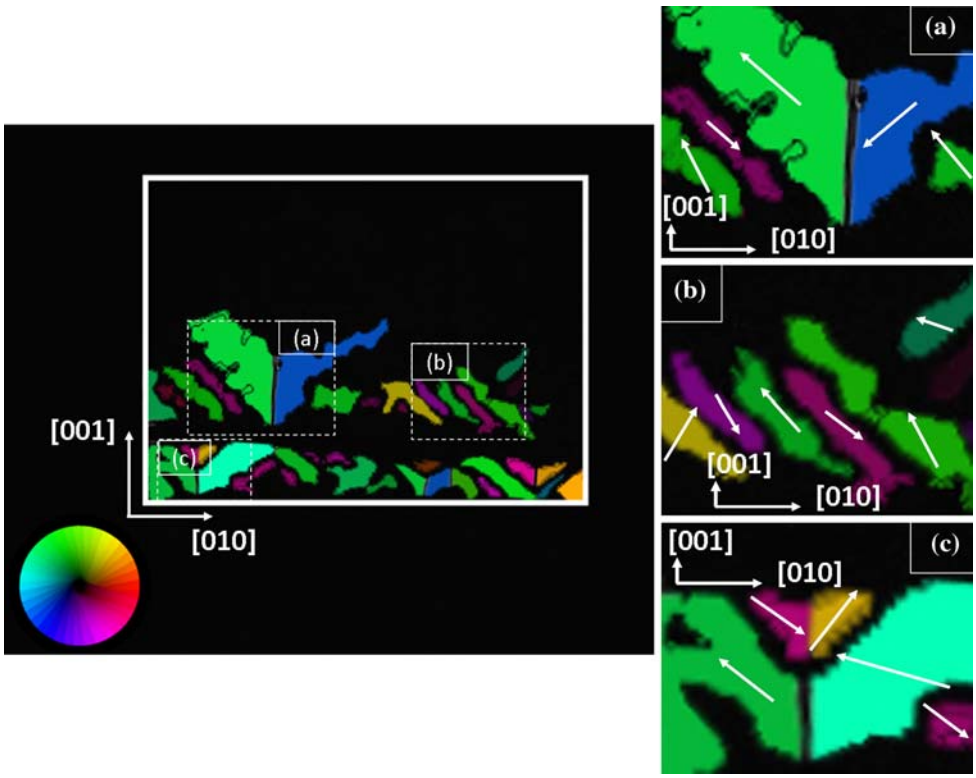

Fig. 5 Full presentation of the local resultant in-plane polarisation through a vector PFM map, and blow-up regions labelled **a**, **b** and **c**. The white rectangle marked on the left-hand overview map marks the approximate outline of the $BaTiO_3$ lamella. Colours indicate the direction of the resultant in-plane component inferred through the lateral PFM measurements. Brightness correlates with the magnitude of the vector. For clarity, we have plotted arrows onto each domain region, with the direction and length of the arrows indicating the direction and magnitude of the local resultant vector PFM signal. Clearly, implied local in-plane polarisations are unphysical, as they are not parallel to the known $[100]_{psuedocubic}$ crystallographic directions

so another resolution statement can be made that $\tau_{LiA} < t$ for the features to be completely resolved. In simple terms, the distance over which the tip moves in the integration time period must be shorter than the distance between features, for those features to be resolved completely. In summary, the limit to resolution in large size PFM scans will be the larger of the two expressions: $d = 2\tau_{LiA}LF_{scan}$ and $d = \frac{L}{N_s}$.

The apparent unphysical polar orientations of $<110>_{pseudocubic}$ inferred from the lateral PFM images in Fig. 4, could have arisen due to the resolution being insufficient to sample individual 90° domains. Instead a number of 90° domains could be sampled simultaneously for any given pixel, yielding resultant (spatially averaged) force interactions along $<110>_{pseudocubic}$. One concern is then that packets of 90° stripe domains would always need to have $\{110\}_{pseudocubic}$ boundaries to be consistent with all the PFM images. Previous STEM imaging on $BaTiO_3$ lamellae shows clearly that boundaries between packets of 90° stripe domains can be of {110} type, but are also regularly observed to be of {100} type (see Fig. 6). So, while it is possible that relatively poor resolution could lead to the in-plane vector PFM information found, the case is not conclusive.

Conclusions

In conclusion, piezo-force microscopy (PFM) of single crystal $BaTiO_3$ lamellae has been performed, and results have been compared to those obtained by scanning transmission electron microscopy (STEM) investigations. Distinct differences in domain widths measured from PFM and STEM images suggested that the differences in imaging conditions result in a ~100-fold change in surface energy densities. Both techniques revealed the same orientations of domain walls, implying in both cases that local polarisations lay in the plane of the lamellae, with 90° rotations of polar orientations between adjacent domains. However, attempts at vector PFM, using the assumptions and simplifications used in the majority of PFM studies in the literature, revealed contradictions between information obtained and the local polarisations allowable given the symmetry of the $BaTiO_3$ and the orientation in which the lamellae had been cut.

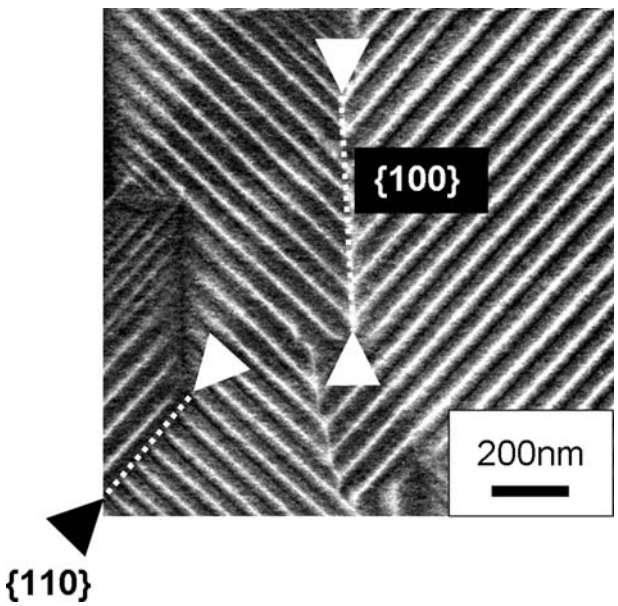

Fig. 6 STEM images on thin lamellae frequently show 90° stripe domains forming into packets. Within each packet, a space-averaged polar orientation would be of type $<110>_{pseudocubic}$, rather than $<001>_{pseudocubic}$, which could be consistent with in-plane vector PFM data in which spatial resolution is below that needed to resolve individual stripe domains. However, this interpretation would demand that the boundaries between packets of stripe domains should all lie parallel to $\{110\}_{pseudocubic}$, given the PFM images in Figs. 2, 3, 4. Clearly, as illustrated in this STEM image, packet boundaries parallel to both $\{100\}_{pseudocubic}$ and $\{110\}_{pseudocubic}$ are commonly observed

Acknowledgements The authors wish to acknowledge discussions and assistance from S. Kalinin and his research group at OakRidge National Labs, as well as Prof J. F. Scott and Dr G. Catalan from the University of Cambridge. Financial support from the UK funding agencies EPSRC and DEL is acknowledged.

References

1. International Technology Roadmap for Semiconductors (ITRS), 2006 Update (2006) p 23. http://www.itrs.net/Links/2006Update/2006UpdateFinal.htm
2. Naber RCG, Tanase C, Blom PWM, Gelinck GH, Marsman AW, Touwslager FJ, Setayesh S, De Leeuw DM (2005) Nat Mat 4:243
3. Tokumitsu E, Fujii G, Ishiwara H (1999) Appl Phys Lett 75:575
4. Landau L, Lifshitz E (1935) Phys Z Sowjetunion 8:153
5. Kittel C (1946) Phys Rev 70:965
6. Roytburd AL (1976) Phys Status Solidi A 37:329
7. Fong DD, Kolpak AM, Eastman JA, Streiffer SK, Fuoss PH, Stephenson GB, Thompson C, Kim DM, Choi KJ, Eom CB, Grinberg I, Rappe AM (2006) Phys Rev Lett 96:127601
8. Schilling A, Adams TB, Bowman RM, Gregg JM, Catalan G, Scott JF (2006) Phys Rev B 74:024115
9. Schilling A, Bowman RM, Catalan G, Scott JF, Gregg JM (2007) Nano Lett 7(12):3787
10. Schilling A, Bowman RM, Gregg JM, Catalan G, Scott JF (2006) Appl Phys Lett 89:212902
11. Catalan G, Schilling A, Scott JF, Gregg JM (2007) J Phys Condens Matter 19:132201
12. Schilling A, Byrne D, Catalan G, Weber K, Genenko Y, Scott JF, Gregg JM (2009) Nano Lett (submitted)
13. Luk'yanchuk IA, Schilling A, Gregg JM, Catalan G, Scott JF (2009) Phys Rev B 79:144111
14. Eng LM, Güntherodt HJ, Rosenman G, Skliar A, Oron M, Katz M, Eger D (1998) J Appl Phys 83:5973
15. Rosen CZ, Hiremath BV, Newnham R (eds) (1992) Piezoelectricity. American Institute of Physics, Key Papers in Physics, No 5, 227
16. Kalinin SV, Rodriguez BJ, Jesse S, Shin J, Baddorf AP, Gupta P, Jain H, Gruverman A, Williams DB (2006) Microsc Microanal 12:206
17. Eng LM, Guntherodt H-J, Schneider GA, Kopke U, Munoz Saldana J (1999) Appl Phys Lett 74:2
18. Rodriguez BJ, Gruverman A, Kingon AI, Nemanich RJ, Cross JS (2004) J Appl Phys 95:4
19. Kalinin SV, Bonnell DA (2002) Phys Rev B 65:125408

20. Kalinin SV, Karapetian E, Kachanov M (2004) Phys Rev B 70:184101
21. Huey BD, Ramanujan C, Bobji M, Blendell J, White G, Szoszkiewicz R, Kulik A (2004) J Electroceram 13:287
22. Saad MM, Baxter P, Bowman RM, Gregg JM, Morrison FD, Scott JF (2004) J Phys Condens Matter 16:L451
23. Wang RV, Fong DD, Jiang F, Highland MJ, Fuoss PH, Thompson C, Kolpak AM, Eastman JA, Streiffer SK, Rappe AM, Stephenson GB (2009) Phys Rev Lett 102:047601
24. Salehi-Khojin A et al (2009) J Sound Vib 322:1081. doi: 10.1016/j.jsv.2008.11.039
25. Harnagea C, Martin F, Legare F, Pignolet A (in preparation)